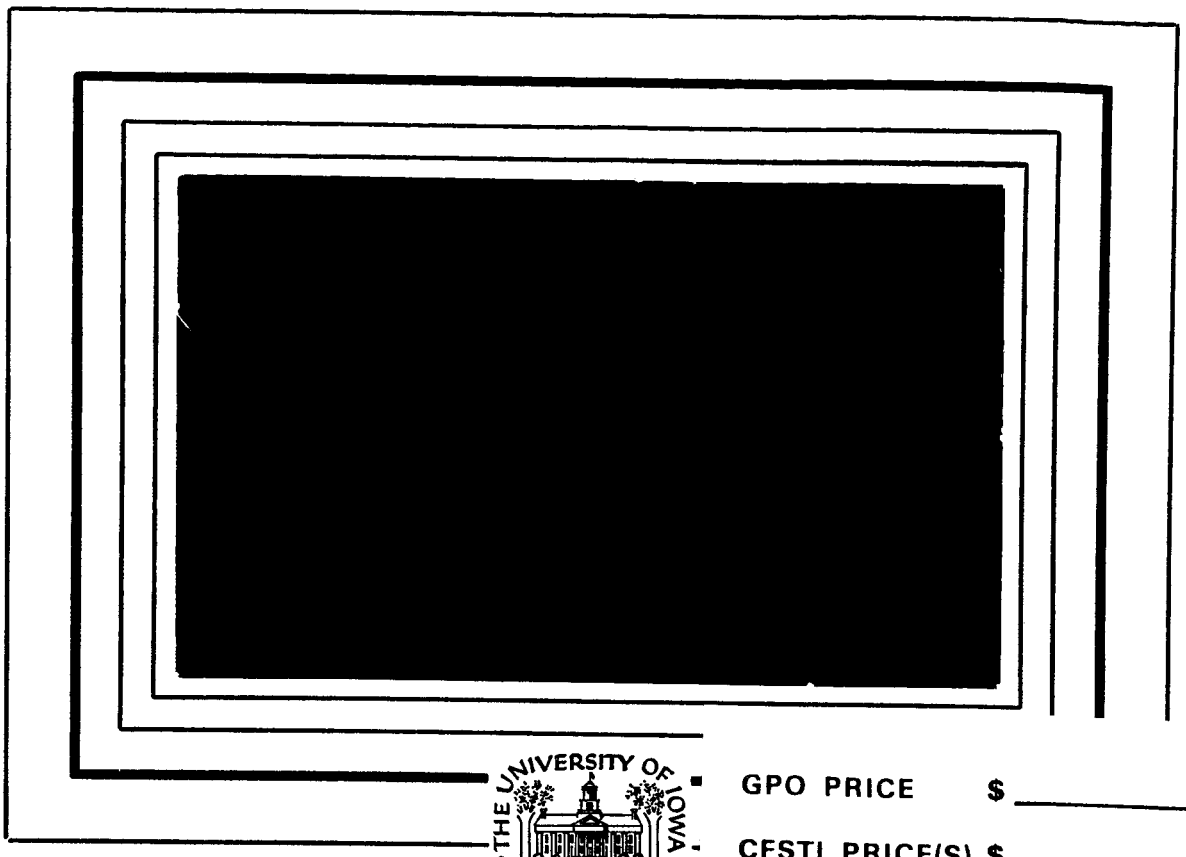

This work was supported in part by the office of Naval Research under Contract No. Nonr-1509(06)

Department of Physics and Astronomy
THE UNIVERSITY OF IOWA
Iowa City, Iowa

INITIAL OBSERVATIONS OF LOW-ENERGY ELECTRONS IN THE EARTH'S MAGNETOSPHERE WITH OGO 3*

by

L. A. Frank

Department of Physics and Astronomy
University of Iowa
Iowa City, Iowa

August 1966

*Research supported in part by the National Aeronautics and Space Administration under Grant NsG-233-62 and Contract NAS5-2054 and by the Office of Naval Research under Contract Nonr-1509(06).

Abstract

Initial observations of electrons over the energy range extending from ~ 100 eV to 50 keV at geocentric radial distances 8 R_E to 20 R_E in the dark hemisphere of the earth's magnetosphere with electrostatic analyzers borne on OGO 3 (launch, 7 June 1966) are presented for the inbound pass of the satellite on 12-13 June 1966. The electron differential energy spectrums typically are characterized by a single peak in intensities occurring in the energy range ~ 0.8 to 10 keV and at lower energies with increasing geocentric radial distance, by broader widths with decreasing radial distance, and by greater slopes for electron energies $E_e \gtrsim 5$ keV with increasing radial distance. The radial profiles of unidirectional and omnidirectional, integral and differential intensities, and energy densities of electrons within the above energy range are characterized by catastrophic variations in magnitude which are presumably reflections of both temporal and spatial variations in intensities. A relatively uncommon example of an electron spectrum with two peaks in intensities at $E_e \simeq 1$ keV and $\simeq 10$ keV is examined during the onset of the event and the peaks in electron intensities were found to occur

at lower energies with increasing time. Beyond ~ 13 R_E many electron spectrums are 'monoenergetic' to the extent that $\gtrsim$ 75% of the energy flux is shared among electrons in the energy range 1 to 3 keV, as an example, although measurable electron intensities are observed over the entire energy range ~ 400 eV to 50 keV. In contrast with the persistent softening of the electron spectrums with increasing radial distance 8 R_E to 20 R_E, the electron energy densities in the peaks of intensities do not show a marked radial dependence beyond ~ 13 R_E. The observed electron (E_e > 280 eV) energy densities in the peaks of the radial profiles almost always rise to ~ 10^{-9} erg(cm)$^{-3}$, an effect which may be indicative of an instability or 'saturation' of the local magnetic field, and are significant in substantially distorting the geomagnetic field beyond ~ 8 R_E. Typical values of the ratios of intensities $J(E_e > 610 \text{ eV})/J(E_e > 45 \text{ keV})$ are 10^4 in the magnetospheric tail. The maximum temporal resolution of the apparatus is ~ 100 milliseconds: temporal variations of low-energy electron intensities by factors $\gtrsim$ 2 occurred usually in periods ~ seconds to several minutes.

I. Introduction

Observations of electrons over an energy range extending from approximately 1 eV to 1 MeV in the distant magnetosphere have already been provided with satellite-borne plasma cups, Geiger-Mueller tubes, electrostatic analyzers, scintillators and solid state devices. Although many of these experiments lacked the temporal resolution, energy discrimination and range, spatial coverage or sensitivity to provide comprehensive information concerning the character of the low-energy electron distributions in the distant magnetosphere (the transition region, the magnetopause, and the earth's magnetic tail), our present knowledge of these electron distributions is sufficient for discerning several of the magnetospheric phenomena and for providing important information in the design of future experiments directed toward more detailed investigations of magnetospheric processes. Several of these surveys of electrons have been reported by Serbu and Maier [1966] over the energy range 0 eV to 50 eV, by Gringauz and his collaborators [1960; 1963], Freeman [1964], and Bridge and his

associates [1965] over the energy range ~ 50 eV to a few kiloelectron volts, and by Frank [1965a, b], Anderson [1965], Frank and Van Allen [1964], Pizzella, Davis and Williamson [1966], and Serlemitsos [1966] over the energy range ~ 10 keV to 1 MeV. Observations of low-energy electrons at geocentric radial distances ~ 17 R_E (R_E, earth radius) with good energy resolution over a substantial portion of the above energy range, 350 eV to 20 keV, with the Vela satellites have been summarized by Coon [1966]. The following presentation is directed toward examining the electron spectrums and intensities over the energy range extending from ~ 100 eV to 50,000 eV from 8 R_E to 20 R_E geocentric radial distances in the dark hemisphere of the magnetosphere with initial measurements obtained with cylindrical-plate electrostatic analyzers borne on the satellite OGO 3.

II. Description of Apparatus

OGO 3 (1966-49A) was launched at 02:48 U.T. on 7 June 1966 into a highly eccentric orbit with initial apogee 128,500 km and perigee 6,700 km geocentric radial distances, inclination 31° and period 48.6 hours. At launch the local time of the direction of the line of apsides was ~ 22:00. A composite system of reaction wheels and gas jets provided a predetermined, monitored orientation of the various spacecraft coordinates with respect to the directions from the satellite to earth and the sun and with respect to the orbital plane. This attitude system operated normally from launch to 23 July 1966. On 23 July a power inverter associated with the attitude control system failed and the spacecraft was subsequently commanded into a spin-stabilized mode. All data presented here were acquired during the period of normal operation of the attitude system.

The University of Iowa instrumentation includes four cylindrical-plate electrostatic analyzers to select charged particle energy and continuous channel multipliers (Bendix 'channeltrons') as charged particle detectors. Each of the two pairs of electrostatic analyzers provides simultaneous

measurements of the intensities of protons and electrons, separately, with the same energy over an energy range extending from ~ 100 eV to 50,000 eV. The directions of the fields of view of these two pairs of electrostatic analyzers, designated as LEPEDEA's 'A' and 'B', are orthogonal and are directed parallel to spacecraft body Cartesian axes, + Z (toward earth in normal satellite operations) and + Y, respectively. Two EON type 213 Geiger-Mueller tubes (1.2 $mg(cm)^{-2}$ mica windows) were positioned in the instrument package such that the directions of their collimated fields of view were parallel to those of the two electrostatic analyzer pairs. The unidirectional geometric factor of these G.M. tubes is 1.5×10^{-3} cm^2 sr; the corresponding half-angle of their conical fields of view is 15°. Penetrating particle energy thresholds within these fields of view are $E_e \simeq 45$ keV and $E_p \simeq 500$ keV. All of the experiment detectors and electronics including eight high-voltage power supplies ($\geq$ 1 kilovolt), four electrostatic analyzers, two Geiger-Mueller tubes, a signal processor and a power converter were mounted in a container on the spacecraft EP-2 appendage (a short boom) with a total weight 6.3 lbs. and power consumption 2.5 watts. The entire instrumentation

has operated satisfactorily from experiment turn-on on 9 June to the present date (1 August 1966).

A diagram of the salient mechanical features of one of the two identical Low Energy Proton and Electron Differential Energy Analyzers (abbreviation, LEPEDEA) is shown in Figure 1 (for more details concerning this instrumentation, see Frank [1965c]). Three cylindrical curved plates P_1, P_2 and P_3 are used to form two 43° electrostatic analyzers for determination of proton and electron differential energy spectrums separately. The two outer plates P_1 and P_3 are tied to circuit ground and the center plate P_2 is biased with a variable positive potential ranging from approximately 0.5 volt to 4.5 kilovolts. Hence the outer analyzer C_2 accepts electrons of appropriate energy and the inner analyzer C_1 performs simultaneous analyses of positive ion differential energy spectrums. This geometry was chosen primarily because of its mechanical simplicity (only one curved plate with high voltage is required for two electrostatic analyzers), large energy bandpass width and large geometric factor. The radii of curvature for plates P_1, P_2 and P_3 are 11.6 cm, 12.8 cm and 13.9 cm, respectively. In order to suppress

the ultraviolet and electron scattering along the analyzer plates into the particle detectors the concave surfaces of plates P_2 and P_3 were machined with sawtooth serrations 1 mm in depth and facing the entrance apertures of the electrostatic analyzers. An elaborate collimator with knife-edged light baffles was also added to reduce this scattering and to define an approximately rectangular field of view with dimensions 6° and 22° in the plane of and in the plane perpendicular to Figure 1, respectively. All interior surfaces of the electrostatic analyzers and the collimator were platinum-blackened to further suppress the detector response to solar ultraviolet emissions. During the period of observations reported here no evidence for a measurable detector response to ultraviolet light has been found.

A simplified diagram of the mounting of the continuous channel multipliers is also shown in Figure 1. The multipliers are positioned such that the normals to the surfaces of their entrance apertures form approximately a 30° angle with the normals to the exit apertures of their associated electrostatic analyzers. This geometry forces all primary charged particles incident on the aperture of the multiplier

to produce secondary electrons near the front end (as compared with normal incidence where primary particles could penetrate more deeply into the throat of the multiplier before striking the capillary wall) thus utilizing the full gain of the detector without a large sacrifice in projected area. The entrance apertures of the continuous channel multipliers are biased with 150 volts (A) and -3 kilovolts (B) for post-acceleration of electrons and protons, respectively [Frank, 1965c]. Electron pulses arriving at the exit apertures, C and D, of the multipliers are accelerated into charge-collecting cups, Y and X, by a potential difference of + 50 volts. The cup Y for the electron channel is biased with +3 kilovolts and is coupled into a voltage-sensitive pulse amplifier with a capacitor.

The voltages on the curved plates of the electrostatic analyzers are incremented once each 18.9 seconds over a voltage range extending from approximately 0.5 volt to 4.5 kilovolts in a predetermined and monitored sequence of 15 steps followed by a scanning mode of duration 18.9 seconds during which the plate voltage monotonically decreases from 4.5 kilovolts to 0.5 volt. During the stepped-voltage mode

the energy resolution of the electrostatic analyzers, $\Delta E/E \simeq 0.5$, is sufficient to span without gaps in particle energy the entire energy ranges for protons and electrons, 100 eV $\leq E \leq$ 50 keV, in thirteen steps. Exemplary results of the laboratory calibrations of LEPEDEA 'B' electron channels are shown in Figure 2 which displays the coverage of the electron energy decade 1 keV to 10 keV provided by five consecutive voltage steps on the electrostatic analyzer. A beam of electrons with constant intensity (5×10^5 electrons $(cm^2\text{-sec})^{-1}$), angle of incidence $\theta = 5°$ and variable energy was used to scan these five adjacent energy bandpasses. (The angle of incidence, θ, is defined as the angle between the normal to the entrance aperture of the electrostatic analyzer and the direction of the charged particle beam. This angle lies in the plane of Figure 1 and is positive to the right.) The bandpasses are well-defined with background rates due to electron scattering smaller than the peak bandpass response by a factor ≥ 500. The gaps between the energy bandpasses shown in Figure 2 are filled by the dispersion of these bandpasses as a function of incidence angle θ (see Figure 3 for typical dispersion in one energy bandpass).

Energy bandpasses for LEPEDEA 'B' electron channels are summarized in Table I. Only observations with the LEPEDEA 'B' electron electrostatic analyzer are presented in this initial study. Descriptions of the remaining three electrostatic analyzers will be provided in subsequent investigations. The geometric factors and energy bandpasses of these electrostatic analyzers have been calculated from detailed laboratory calibrations such as those shown in Figure 3. As examples, the efficiencies of electron channels 6eB and 14eB (Table I) are 1.5 ($\pm$ 0.3) x 10^{-2} and 4.9 ($\pm$ 1.0) x 10^{-1} (count-cm^2-sr-eV) $(electron)^{-1}$, respectively.

All four electrostatic analyzers, two Geiger-Mueller tubes, and curved-plate voltage monitors (a calibration sample for each pair of proton and electron measurements) time-shared the experiment 15-bit accumulator in a complex, but tractable, manner. The contents of this accumulator were telemetered once each 1.15, 0.144 or 0.018 seconds for the three possible spacecraft data rates, 1, 8 or 64 kilobits $(sec)^{-1}$. Experiment data tapes were subsequently provided by the Goddard Space Flight Center for analysis at the University of Iowa. This analysis included identification of the 68 channels of information which had been subcommutated

TABLE I

OGO 3 LEPEDEA ELECTRON CHANNELS 'B'
ENERGY BANDPASSES

Electron Channel	Energy Bandpass*
3eB	80 - 140 eV
4eB	170 - 300 eV
5eB	280 - 500 eV
6eB	380 - 680 eV
7eB	610 - 1100 eV
8eB	940 - 1700 eV
9eB	1.5 - 2.7 keV
10eB	2.8 - 5.0 keV
11eB	4.1 - 7.2 keV
12eB	5.8 - 10 keV
13eB	9.8 - 17 keV
14eB	14 - 24 keV
15eB	26 - 46 keV

*Analyzer constant is 7.3 ev(volt)$^{-1}$.

into two 9-bit spacecraft telemetry words, elimination of noisy data, merging the orbital information with the experiment data, and calculations of proton and electron differential (and integral) energy spectrums, energy densities and individual energy bandpass intensities.

III. Observations

The responses of two LEPEDEA 'B' electron channels, 9eB and 14eB, and of the 213B G.M. tube are shown in Figure 4 as a function of geocentric radial distance for the inbound pass of 12-13 June 1966. All data for these detectors during this period of observations are not shown in these graphs; the sampling density displayed in Figure 4 is $\sim$ 10 samples $(R_E)^{-1}$. In fact, during this single pass approximately 1.1×10^6 individual measurements of proton and electron intensities and 1.4×10^3 proton and electron spectrums were telemetered by the spacecraft and subsequently processed at the University of Iowa. Several salient features of the electron spectrums and intensities for this single pass are presented in the following graphs. Inspection of Figure 4 clearly indicates (1) the electron spectrums soften with increasing geocentric radial distance, (2) 'spikes' of intensities with larger response amplitudes at lower energy, (3) both positive and no correlations of electron ($1.5 \leq E_e \leq 2.7$ keV) and ($E_e > 45$ keV) intensity variations over the radial distances extending from 8 to 11.5 R_E, and (4) electron ($1.5 \leq E_e \leq 2.7$ keV) intensities at 20 R_E which are

similar in magnitude when compared to intensities found deeper in the magnetosphere at ~ 8 R_E. The daily sums of the planetary magnetic indices K_p were 14o and 10- on 12 and 13 June, respectively [I.U.G.G., Association of Geomagnetism and Aeronomy, Commission No. 4]. Several useful position coordinates of the spacecraft as a function of geocentric radial distance are plotted in Figure 5: solar ecliptic latitude and longitude, θ_{SE} and φ_{SE}; solar magnetospheric latitude, θ_{SM} [Ness, 1965], and geomagnetic latitude λ_m. As shown in Figure 5 OGO 3 crossed the midnight meridional plane at ~ 10.5 R_E at moderate solar ecliptic and magnetospheric latitudes, ~ 35°; geomagnetic latitudes ranged from ~ 6° to 15° over radial distances 8 R_E to 19 R_E. During the period of observations shown in Figure 1 and presented in the following discussion the longitude of the spacecraft position differed from the longitude of the midnight meridional plane by $\leq$ 30°. The directions of the LEPEDEA 'B' axis of its field of view as functions of geocentric radial distance in several coordinate systems are summarized in Table II.

TABLE II

COORDINATES FOR THE AXIS OF LEPEDEA 'B'
FIELD OF VIEW
12-13 JUNE 1966 (INBOUND)
OGO 3

Satellite Position, geocentric radial distance	Axis directed along: Solar-ecliptic θ_{SE}	φ_{SE}	Solar-magnetospheric θ_{SE}^{m}	φ_{SE}^{m}	Pitch angle* (dipole field) α
9 R_E	-57°	171°	-54°	154°	33°
11 R_E	-55°	185°	-54°	165°	29°
13 R_E	-51°	193°	-53°	174°	24°
15 R_E	-48°	198°	-51°	184°	18°
17 R_E	-44°	201°	-46°	197°	18°
19 R_E	-39°	203°	-36°	207°	37°

*Convention: if $\vec{v} \parallel \vec{B}$, $\alpha \equiv 0°$

Omnidirectional intensities of electrons $E_e > 610$ eV and > 5.8 keV as functions of geocentric radial distance are shown in Figure 6. These omnidirectional intensities were calculated by integrating the differential energy spectrums observed with LEPEDEA 'B' and with the assumption of isotropic angular distributions. The assumption of isotropy was corroborated with measurements of electron intensities with LEPEDEA 'A' (axis of 'A' field of view directed perpendicular to that of 'B') to within a factor of ~ 2 for the observations summarized in Figure 6. Peak omnidirectional intensities of electrons $E_e > 610$ eV are $\sim 10^9$ $(cm^2\text{-sec})^{-1}$ from 8 R_E to 20 R_E; intensity variations by factors $\sim 10^3$ are easily discernible beyond ~ 10.5 R_E. Inspection of the peak intensities of electrons $E_e > 5.8$ keV shows a stronger modulation of intensities with increasing radial distance when compared to the lower energy electron intensities, $J_o(> 5.8 \text{ keV}) \simeq 10^9$ $(cm^2\text{-sec})^{-1}$ at 9.5 R_E and $\simeq 4 \times 10^7$ $(cm^2\text{-sec})^{-1}$ at 19.7 R_E. Several of these electron spectrums at larger radial distances are extremely soft. For example, at 17 R_E $J_o(> 610 \text{ eV})/J_o(> 5.8 \text{ keV}) \simeq 300$ whereas at 9.5 R_E this ratio is $\simeq 2$. The threshold intensity for

the detector array in these calculations providing $J_o(> 5.8$ keV) is 3×10^5 $(cm^2\text{-sec})^{-1}$, or $\sim 10^{-3}$ erg$(cm^2\text{-sec})^{-1}$. Electron ($E_e > 280$ eV) energy densities, erg$(cm)^{-3}$, are shown in Figure 7 for this series of observations. Energy densities ranging from $\sim 5 \times 10^{-9}$ to $\sim 10^{-12}$ erg$(cm)^{-3}$ with rapid variations in the radial profiles are easily evident. It is noteworthy that the peaks of energy density from ~ 13 R_E to 20 R_E rise to values $\sim 6(\pm 4) \times 10^{-10}$ erg$(cm)^{-3}$ with a relative absence of smaller maxima in the range $\sim 5 \times 10^{-12}$ to 2×10^{-10} erg$(cm)^{-3}$. An electron energy density $\sim 6(\pm 4) \times 10^{-10}$ erg$(cm)^{-3}$ corresponds to a diamagnetic effect $\simeq 13\gamma$ ($\Delta B = (8 \pi \bar{E})^{1/2}$ where $\bar{E}$ is the electron energy density) which is within a factor of 2 or 3 of the average magnetic field magnitude in the 'tail' region reported by Ness [1965]. At 10 R_E the electron energy density is $\simeq 5 \times 10^{-9}$ erg$(cm)^{-3}$ ($(8 \pi \bar{E})^{1/2} \simeq 35\ \gamma$) and the corresponding magnetic field energy density using an earth-centered dipole approximation, for a comparison only, is 5×10^{-9} erg$(cm)^{-3}$. Clearly the electron energy densities displayed in Figure 7 are important in significantly distorting the geomagnetic field over the radial distance range extending from 8 R_E to 20 R_E.

At 8.5 R_E to 10.5 R_E the omnidirectional electron ($E_e > 610$ eV) intensities $\sim 10^9$ $(cm^2\text{-sec})^{-1}$ and omnidirectional energy fluxes ~ 10 erg$(cm^2\text{-sec})^{-1}$ compare favorably with results reported by Gringauz and his associates [1960, 1963] and Freeman [1964], respectively.

Several exemplary electron spectrums (500 eV $< E_e <$ 50 keV) at selected geocentric radial distances are displayed in Figure 8. These differential energy spectrums typically broaden with decreasing radial distance, become steeper for $E_e \gtrsim 5$ keV with increasing radial distance and are characterized by a peak intensity occurring at lower energies with increasing radial distances. For example, at 19.7 R_E and 13.5 R_E the peak intensities are 5×10^4 electrons $(cm^2\text{-sec-sr-ev})^{-1}$ at $E_e \simeq 1$ keV and 3×10^4 $(cm^2\text{-sec-sr-ev})^{-1}$ at $E_e \simeq 2$ keV, respectively. Electron densities for the electron spectrums at 10.1 R_E, 13.5 R_E and 19.7 R_E shown in Figure 8 are 0.5 ($\pm$ 0.2) electrons $(cm)^{-3}$.

A coarse summary of electron observations for the inbound pass on 12-13 June 1966 has been given in Figures 4 and 6. An example of the detailed character of the responses of LEPEDEA 'B' to a 'spike' or 'island' of electron intensities

[cf. Frank, 1965a; Anderson, 1965] is shown in Figure 9. This 'spike', or 'island', of electron ($E_e > 45$ keV) intensities as observed with the 213B G.M. tube (bottom right-hand corner of Figure 9) is compared with the temporal variations of the LEPEDEA 'B' responses to lower energy electrons in 10 energy bandpasses covering the energy range 380 eV to 46 keV. During this event OGO 3 was at ~ 18 R_E geocentric radial distance and the sun-earth-satellite angle, ψ_{SEP}, was ~ 136°. The duration of this event was ~ 1 hour with largest changes in intensities (by factors ~ 10^3 greater than the detector threshold) occurring over the energy range ~ 1.5 to 5 keV and diminishing amplitudes at lower and higher energies. In fact it is easily noted that 213B G.M. tube responds only to the small, high-energy tail of these electron events. The initial rise of electron intensities occurs in a period of 5 to 10 minutes for all energies shown in Figure 9 with subsequent variations in intensities during the event by factors (energy-dependent) ~ 10 within periods ~ 5 minutes. A search for more rapid temporal variations is discussed later. Another example of these electron spectrums is shown in Figure 10 which features an electron spectrum of different character, a 'plateau' over the energy range 2 to 5 keV, when

compared to the more typical spectrums shown in Figure 8. The corresponding integral spectrum, J(> E), has been included in Figure 10 to demonstrate the relationship of the 213B G.M. tube measurement with the LEPEDEA 'B' electron observations. Note that $J(> 170\ eV) \simeq 5 \times 10^7$ electrons $(cm^2\text{-sec-sr})^{-1}$ and $J(> 45\ keV) \simeq 5 \times 10^3$. Several of the electron intensity 'spikes' shown in Figure 6 beyond $\sim 13\ R_E$ were unobservable with the G.M. tube, or $J(> 45\ keV) \lesssim 10^3\ (cm^2\text{-sec-sr})^{-1}$.

The temporal variations of the electron spectrum shown in Figure 10 during the onset of the event display the remarkable behavior shown in Figure 11. The three differential energy spectrums at 5-minute intervals show clearly that, whereas typically only a single peak in the spectrum appears during the onset, two discernible peaks, at $E_e \sim 1$ keV and $E_e \sim 10$ keV, occur at the same time and 'grow' in a similar manner with the peaks in intensities shifting to lower energies with increasing time.

An initial search for rapid temporal variations in low-energy electron intensities within periods of 100 milliseconds to 10 seconds indicates that, although rapid fluctuations in intensities by factors $\gtrsim 2$ have been observed within the abridged body of observations shown in Figure 6, typical observations

show a general lack of such temporal features and are illustrated by the segment of data displayed in Figure 12. One average measurement of electron ($1.5 < E_e < 2.7$ keV) intensities shown in Figure 4 at 19.7 R_E has been expanded into its telemetered high-density sample displayed in Figure 12. The sampling density shown in the bottom of Figure 12 is one accumulation of the detector response for a period 17.7 milliseconds with a repetition period 144 milliseconds. Also shown in Figure 12 are corresponding ten-sample, or 1.44 second, averages and the calculated standard deviations for the 17.7 millisecond samples and the averages. Temporal variations in periods 100 milliseconds to 10 seconds by factors $\lesssim 2$ are consistent with the calculated standard deviations of the samples. Hence the 'spikes' of intensities shown in Figure 4 are typified by a general lack of electron intensity pulses (by factors $\gtrsim 2$ in intensity) at peak intensities on time scales ~ 100 milliseconds to ~ seconds and during onset 'grow' within periods ~ minutes to peak intensities over the energy range extending from ~ 400 eV to 50 keV (cf. Figure 9). Exceptions to this initial survey of temporal intensity variations will be discussed in a comprehensive study now in progress.

IV. Summary and Discussion

Initial observations of low-energy electrons over the energy range extending from ~ 100 eV to 50 keV in the dark hemisphere of the magnetosphere from 8 R_E to 20 R_E during 12-13 June 1966 with the satellite OGO 3 have been summarized in the preceding presentation of experimental results. The system of electrostatic analyzers borne on this spacecraft is capable of measuring the electron (and proton) differential energy spectrums over the above energy range with good energy resolution and threshold intensity in two mutually orthogonal directions. With these differential energy spectrums as basic data, corresponding integral spectrums, energy densities, energy fluxes and number densities have been calculated and provided for comparison with other observations. Several of the salient features of the electron distributions reported here deserve further discussion.

As the geocentric radial distance of the observation decreases, electron differential energy spectrums typically harden for $E_e \gtrsim 5$ keV, broaden, and are characterized by a peak in intensities which, in an average sense, occurs at higher energies (see Figures 6 and 8). These results suggest

that the process for accelerating these electrons is effective over a region in the magnetospheric tail extending from at least ~ 10 R_E to 20 R_E. In a rather primitive point of view the persistent average shift of the spectrum peak by several kiloelectron volts over a radial span of ~ 10 R_E would support the existence of an electric field ~ $(5 \times 10^3$ volts$)$ $(10\ R_E)^{-1}$ $\simeq$ 100 millivolts $(km)^{-1}$ in this region. The measurements of electron intensities reported here are in substantial agreement with Vela satellite observations at ~ 17 R_E [Bame, Ashbridge, Felthauser, Olson and Strong, 1966]. At geocentric radial distances ~ 8 R_E to 10 R_E an electron (E_e > 610 eV) intensity ~ $10^9 (cm^2\text{-sec})^{-1}$ and an electron (E_e > 610 eV) energy flux ~ 10 $ergs(cm^2\text{-sec})^{-1}$ are observed. These results compare favorably with results reported by Gringauz [1960, 1963] and Freeman [1964] at this general location within the magnetosphere; a typical electron spectrum is shown at the bottom of Figure 8. It is of further interest to note that the energy flux in the electron spectrums at $\gtrsim$ 13 R_E (refer to Figure 8) is concentrated within a relatively small energy range. For example, approximately 75% of the energy flux for the spectrum at 19.7 R_E shown in Figure 8 is shared by electrons in the narrow energy range 1 to 3 keV

although the measurable spectrum extends from 380 eV to 46 keV. These 'monoenergetic' fluxes of electrons are reminiscent, and indeed are probably the high-altitude counterpart, of rocket measurements of nearly monoenergetic (~ 6 keV) electron fluxes at auroral altitudes [McIlwain, 1960].

Measurements of the low-energy component (see Figure 9) of the 'spikes' or 'islands' of electron(E_e > 45 keV) intensities observed with thin-windowed G.M. tubes [cf. Frank, 1965a; Anderson, 1965] show that (1) the G.M. tubes respond only to the high-energy tail of the electron spectrums, (2) typically the peaks in the electron differential energy spectrums associated with these intensity 'spikes' are in the energy range 0.8 to 10 keV, and (3) J(> 610 eV)/J(> 45 keV) ~ 10^4 for these events. During several substantial electron events as observed with the electrostatic analyzer the 213 G.M. tube (E_e > 45 keV) response remained at background levels. Typical differential energy spectrums beyond ~ 13 R_E can be described by a power law, kE^{-n}, where n = 3($\pm$ 1) for $E_e \gtrsim 5$ keV. An unusual electron spectrum with two peaks in intensities at E_e ~ 1 keV and ~ 10 keV has been reported here (Figure 11). The intensities in both peaks simultaneously increased over

a period ~ 10 minutes during which both peak intensities shifted toward lower energies as the event progressed. The simultaneity and similar temporal behavior of these two intensity peaks suggest that these electrons share a common origin and hence that the acceleration mechanism is sometimes capable of providing at least two electron beams with characteristic energies differing by a factor ~ 10. The most frequently observed electron spectrums beyond ~ 13 R_E possess a single peak in the energy range ~ 0.8 keV to 3 keV. A comprehensive survey of the temporal behavior of these electron spectrums and the companion proton spectrums over the same energy range is now being prepared.

It is easily noted that the radial profiles of low-energy electron intensities are characterized by large, catastrophic decreases and increases in intensities beyond ~ 10 R_E (see, for example, Figure 6). The structure of these intensity profiles is presumably a reflection of a combination of spatial and temporal variations in intensities as seen at the satellite position. The radial profile of the electron (E_e > 280 eV) energy densities shown in Figure 7 provides further information concerning the nature of these 'spikes' of electron intensities; (1) the peak energy densities are

$\sim 10^{-9}$ erg(cm)$^{-3}$ (equivalent diamagnetic effect, $\Delta B = (8 \pi \bar{E})^{1/2} \simeq 15\gamma$), (2) there is a notable relative absence of peaks in the energy density in the range 5×10^{-12} to 2×10^{-10} erg(cm)$^{-3}$, and (3) an absence of a strong radial dependence in the peak energy densities in these spikes within a factor of 2 beyond ~ 13 R_E. In view of these results it is certain that the distribution of electrons as summarized in Figure 7 substantially distorts the geomagnetic field beyond 8 R_E and probable that the persistent peak energy densities $\sim 10^{-9}$ erg(cm)$^{-3}$ beyond ~ 13 R_E reflect a 'saturation' limit of the magnetic field in these regions beyond which the tail field can no longer support the pressure due to the electrons. The relative absence of energy density peaks of smaller amplitude would appear to indicate that the acceleration mechanism drives the electron intensities to this 'saturation' point. It is of further interest to note that the electron energy density peak at ~ 19.5 R_E (Figure 7) was observed while the spacecraft was ~ 12 R_E above the neutral sheet ($\theta_{SM} \simeq 0°$, Ness [1965]). Thus large intensities of low-energy electrons do appear within the earth's magnetic tail at large distances above the neutral sheet (in fact, for this observation, near the midpoint between the position of the neutral sheet and the presumed location of the northern

magnetopause in the meridional cross-section of the magnetosphere [Ness, 1965]). Consideration of these large intensities of electrons at large distances from the neutral sheet in the earth's magnetic tail is important in constructing auroral theories and for analyzing the topology of the magnetic field in the 'tail' region. Observations of large intensities of low-energy electrons at ~ 17 R_E and over broad ranges of θ_{SM} have also been reported by Bame et al [1966] (see also Anderson and Ness [1966] for a comparison of IMP 1 measurements of magnetic field and higher energy, $E_e > 45$ keV, electrons).

Results of an initial investigation of the temporal variations of electron intensities (see Figures 9 and 12) show that the 'spikes' of intensities usually rise in a period ~ minutes and that there are usually no variations of intensities by factors $\gtrsim 2$ in periods ~ 100 milliseconds to ~ several seconds during the peak of intensities. Occasional bursts of electron intensities during these shorter time periods have been observed and will be discussed in a later report. Hence the injection, and perhaps the acceleration, of electrons as seen at the position of the

satellite is characterized in most events by periods ~ a few seconds to several minutes over the energy range extending from ~ 400 eV to 50 keV.

Acknowledgements

The author is indebted to Dr. J. A. Van Allen for his support throughout the various phases of this research. The efforts of D. C. Enemark, N. K. Henderson, R. H. Gabel, W. W. Stanley, R. D. Carlson, R. F. Randall, R. L. Swisher and D. Klumpar during the design and construction phases, L. Shope and C. Brues of the University of Iowa during the computer analysis phase, and Dr. G. H. Ludwig, Dr. E. Mercanti, D. Krueger, E. Moyer and many other members of the Goddard Space Flight Center personnel during the multitudinous phases of spacecraft integration and launch operations are acknowledged with great pleasure.

This research was supported in part by the National Aeronautics and Space Administration under Grant NsG-233-62 and Contract NAS5-2054 and by the Office of Naval Research under Contract Nonr-1509(06).

References

Anderson, K. A., Energetic electron fluxes in the tail of the geomagnetic field, J. Geophys. Res., 70, 4741-4763, 1965.

Anderson, K. A., and N. F. Ness, Correlation of magnetic fields and energetic electrons on the IMP 1 satellite, J. Geophys. Res., 71, 3705-3727, 1966.

Bame, S. J., J. R. Ashbridge, H. E. Felthauser, R. A. Olson, and I. B. Strong, Electrons in the plasma sheet of the earth's magnetic tail, Phys. Rev. Letters, 16, 138, 1966.

Bridge, H., A. Egidi, A. Lazarus, E. Lyon, and L. Jacobson, Preliminary results of plasma measurements on IMP-A, Space Research V, North-Holland Publishing Company, 969-978, 1965.

Coon, James, Vela satellite measurements of particles in the solar wind and the distant geomagnetosphere, Radiation Trapped in the Earth's Magnetic Field, ed. by B. M. McCormac, D. Reidel, 231-255, 1966.

Frank, L. A., A survey of electrons E > 40 keV beyond 5 earth radii with Explorer XIV, J. Geophys. Res., 70, 1593-1626, 1965a.

Frank, L. A., On the local-time dependence of outer radiation zone electron (E > 1.6 MeV) intensities near the magnetic equator, J. Geophys. Res., 70, 4131-4138, 1965b.

Frank, L. A., Low-energy proton and electron experiment for the Orbiting Geophysical Observatories B and E, U. of Iowa Res. Rep. 65-22, 1965c.

Frank, L. A., and J. A. Van Allen, Measurements of energetic electrons in the vicinity of the sunward magnetospheric boundary with Explorer XIV, J. Geophys. Res., 69, 4923-4932, 1964.

Freeman, J. W., The morphology of the electron distribution in the outer radiation zone and near the magnetospheric boundary as observed by Explorer XII, J. Geophys. Res., 69, 1691-1723, 1964.

Gringauz, K. I., V. V. Bezrukikh, L. S. Musatov, R. E. Rybchinsky, and S. M. Sheronova, Measurements made in the earth's magnetosphere by means of charged particle traps aboard the Mars I probe, Space Research, IV, 621-626, 1963.

Gringauz, K. I., V. G. Kurt, V. I. Moroz, and I. S. Shklovskii, Results of observations of charged particles observed

out to R = 100,000 km, with the aid of charged-particle traps on Soviet space rockets, Astron. Zh., 37, 716-735 (1960; translation in: Soviet Astronomy-A.J., 4, 680-695, 1961).

McIlwain, C. E., Direct measurement of particles producing visible auroras, J. Geophys. Res., 65, 2727-2747, 1960.

Ness, N. F., The earth's magnetic tail, J. Geophys. Res., 70, 2989-3003, 1965.

Pizzella, G., L. R. Davis, and J. M. Williamson, Electrons in the Van Allen zone measured with a scintillator on Explorer XIV, Goddard Space Flight Center Preprint, Series X-611-66-112, 1966.

Serbu, G. P., and E. J. R. Maier, Low-energy electrons measured on IMP 2, J. Geophys. Res., 71, 3755-3766, 1966.

Serlemitsos, P., Low-energy electrons in the dark magnetosphere, J. Geophys. Res., 71, 61-77, 1966.

Figure Captions

Figure 1. Diagram of the basic mechanical features of the OGO 3 Low Energy Proton and Electron Differential Energy Analyzer (abbreviation, LEPEDEA).

Figure 2. Laboratory calibrations for five electron channels of LEPEDEA 'B'. The responses of these channels to a directed beam, 5×10^5 electrons$(cm^2\text{-sec})^{-1}$, with fixed angle of incidence $\theta = 5°$ (see text) are plotted as a function of electron energy.

Figure 3. Laboratory calibrations for electron channel 14eB. The responses of this electron channel (fixed voltage on curved plate of the analyzer) to a directed beam, 3×10^5 electrons $(cm^2\text{-sec})^{-1}$, are plotted as a function of electron energy for angles of incidence $\theta = 2°$, $5°$ and $9°$.

Figure 4. The responses of LEPEDEA 'B' channels 9eB and 14eB and of the 213B thin-windowed G.M. tube as functions of geocentric radial distance for the inbound pass of OGO 3 on 12-13 June 1966.

Figure 5. Several useful position coordinates for OGO 3 on 12-13 June 1966 (inbound pass).

Figure 6. Omnidirectional intensities of electrons $E_e > 610$ eV and > 5.8 keV as functions of geocentric radial distance on 12-13 June 1966.

Figure 7. Electron ($E_e > 280$ eV) energy densities as a function of geocentric radial distance on 12-13 June 1966.

Figure 8. Representative electron differential energy spectrums at several geocentric radial distances.

Figure 9. Temporal profiles of the LEPEDEA 'B' responses to electrons (380 eV $< E_e < 46$ keV) intensities during a 'spike', or 'island', event observed with the 213B G.M. tube ($E_e > 45$ keV) at ~ 18 R_E.

Figure 10. Differential and integral energy spectrums for a 'spike', or 'island', of electron intensities rich in higher energy (5 to 10 keV) electron intensities.

Figure 11. Differential energy spectrums at the onset of a 'double-peaked' electron event observed at 15.3 R_E.

Figure 12. An example of LEPEDEA 'B' responses to electron ($1.5 \leq E_e < 2.7$ keV) intensities at maximum temporal resolution during the peak intensities of an electron event observed at 19.7 R_E.

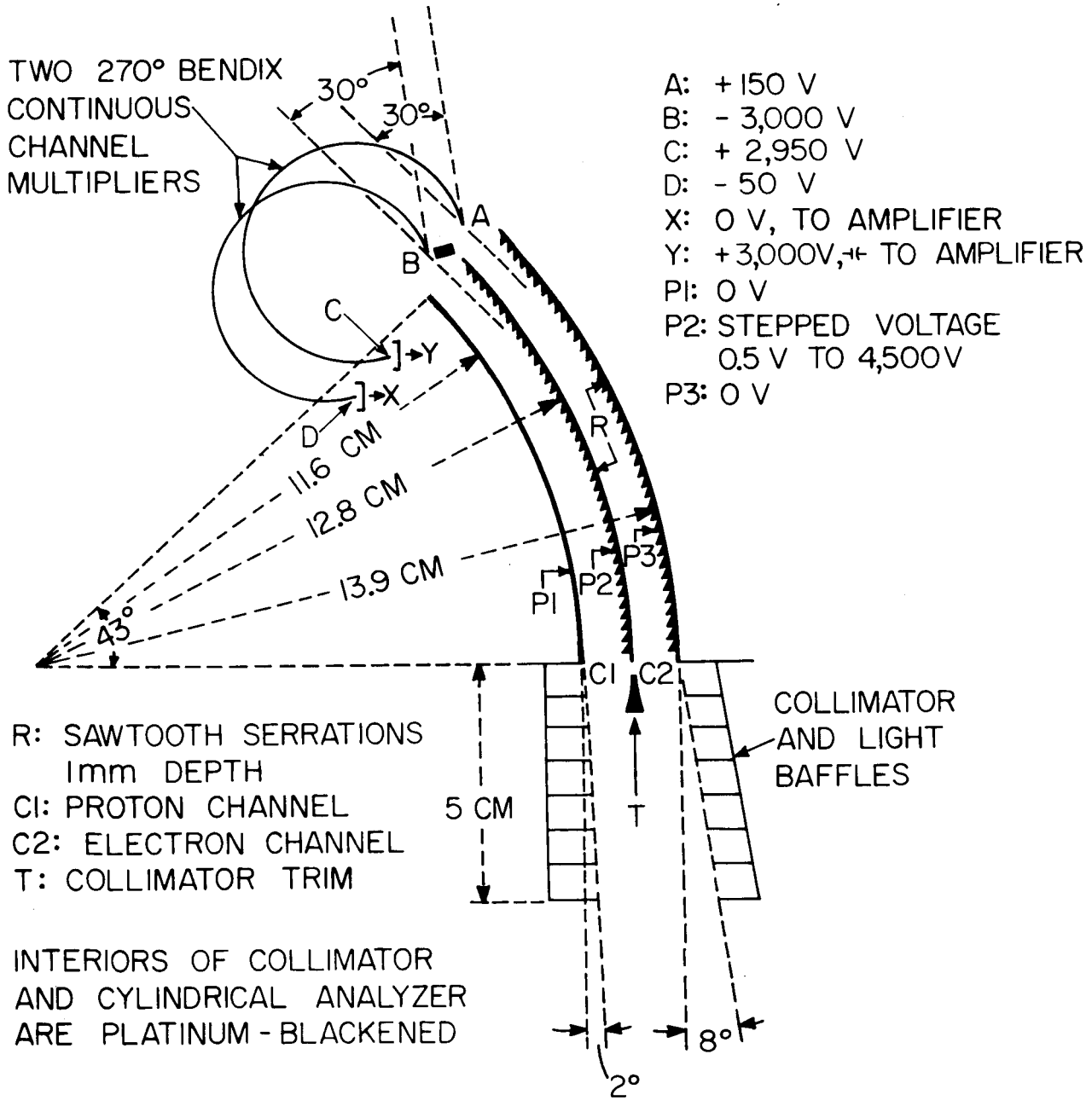
TWO 270° BENDIX CONTINUOUS CHANNEL MULTIPLIERS
30°
30°
A
B
C
]→Y
]→X
D
11.6 CM
12.8 CM
13.9 CM
43°
R
P1
P2
P3
C1
C2
T
5 CM
8°
2°
A: + 150 V
B: - 3,000 V
C: + 2,950 V
D: - 50 V
X: 0 V, TO AMPLIFIER
Y: + 3,000V, TO AMPLIFIER
P1: 0 V
P2: STEPPED VOLTAGE 0.5 V TO 4,500V
P3: 0 V
R: SAWTOOTH SERRATIONS 1mm DEPTH
C1: PROTON CHANNEL
C2: ELECTRON CHANNEL
T: COLLIMATOR TRIM
INTERIORS OF COLLIMATOR AND CYLINDRICAL ANALYZER ARE PLATINUM - BLACKENED
COLLIMATOR AND LIGHT BAFFLES

Figure 1

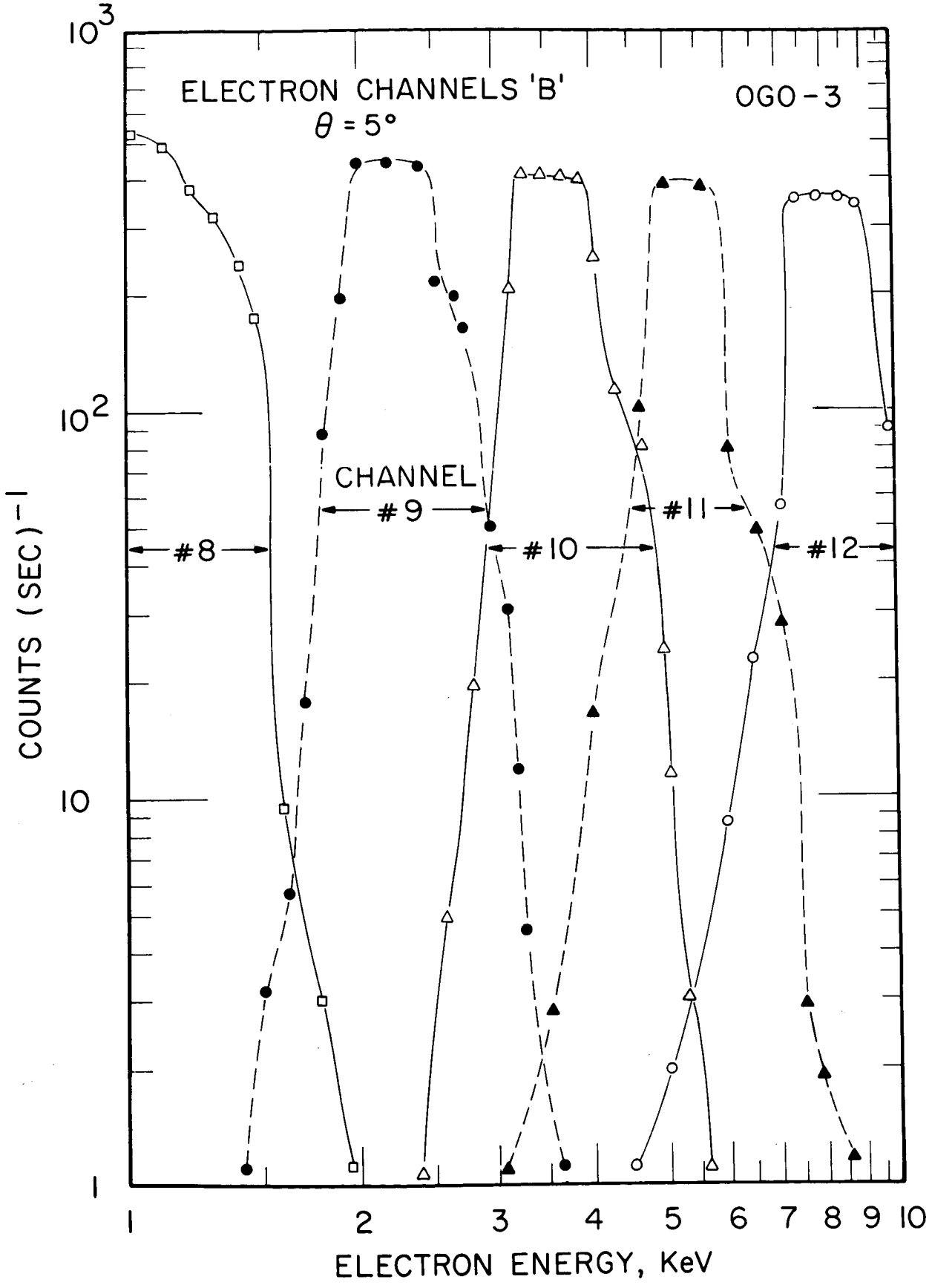
ELECTRON CHANNELS 'B'
θ = 5°
OGO-3
CHANNEL
#8
#9
#10
#11
#12
COUNTS (SEC)⁻¹
10³
10²
10
1
1
2
3
4
5
6
7
8
9
10
ELECTRON ENERGY, KeV

Figure 2

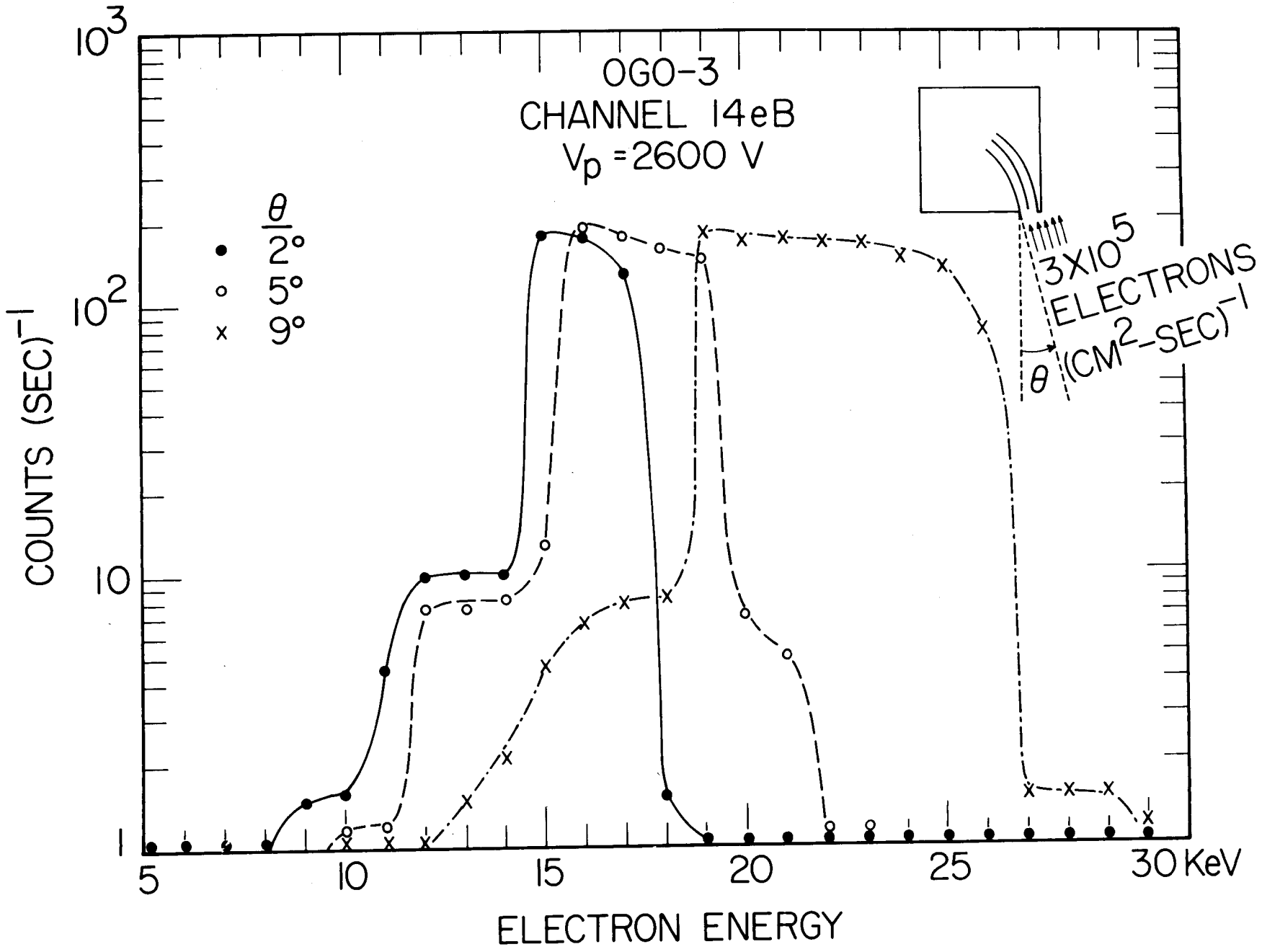
OGO-3
CHANNEL 14eB
V_p = 2600 V
θ
2°
5°
9°
3X10^5 ELECTRONS (CM^2-SEC)^-1
θ
COUNTS (SEC)^-1
10^3
10^2
10
1
5
10
15
20
25
30 KeV
ELECTRON ENERGY

Figure 3

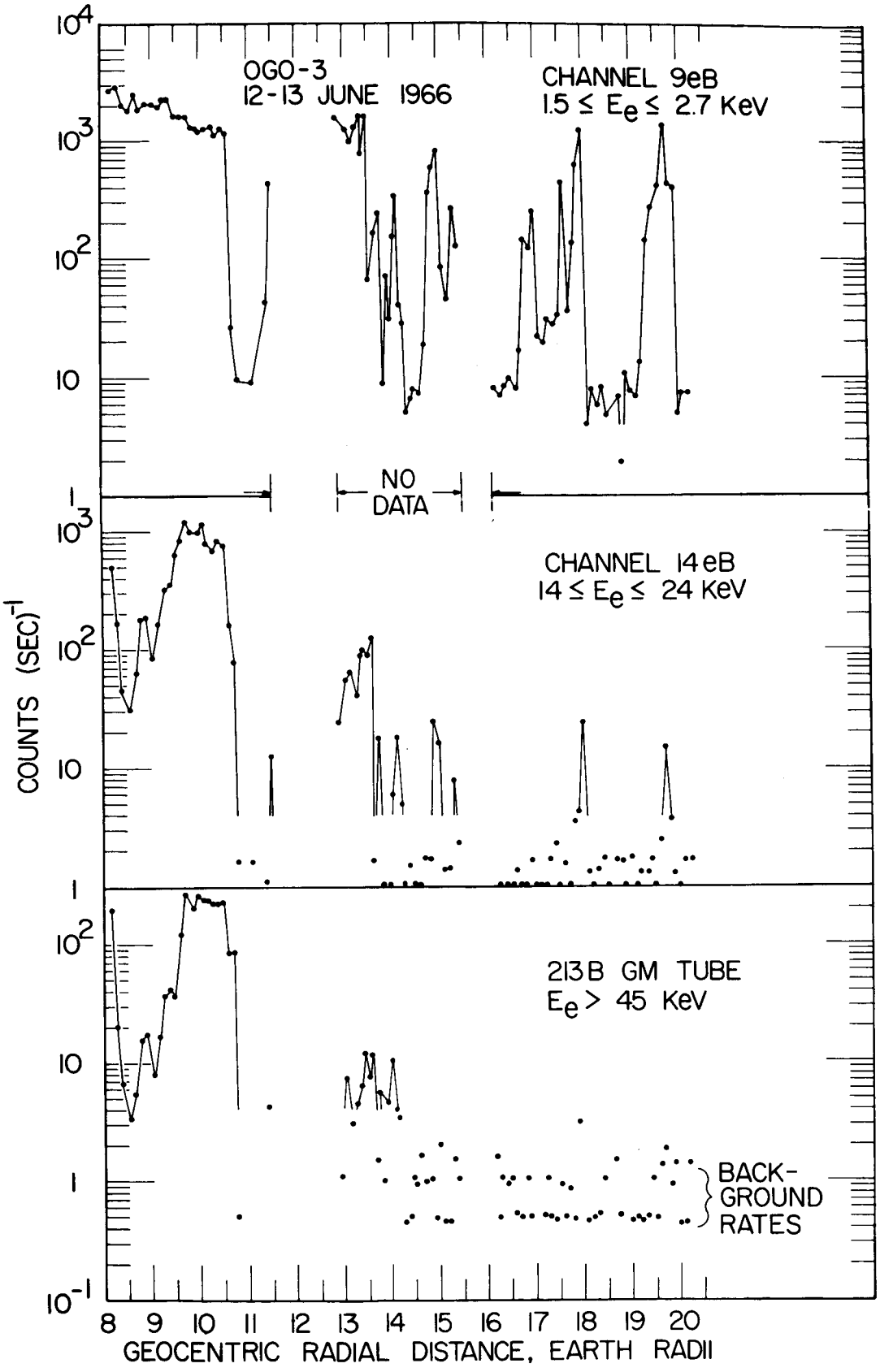
OGO-3
12-13 JUNE 1966
CHANNEL 9eB
1.5 ≤ Ee ≤ 2.7 KeV
NO DATA
CHANNEL 14eB
14 ≤ Ee ≤ 24 KeV
213B GM TUBE
Ee > 45 KeV
BACK-GROUND RATES
COUNTS (SEC)-1
GEOCENTRIC RADIAL DISTANCE, EARTH RADII

Figure 4

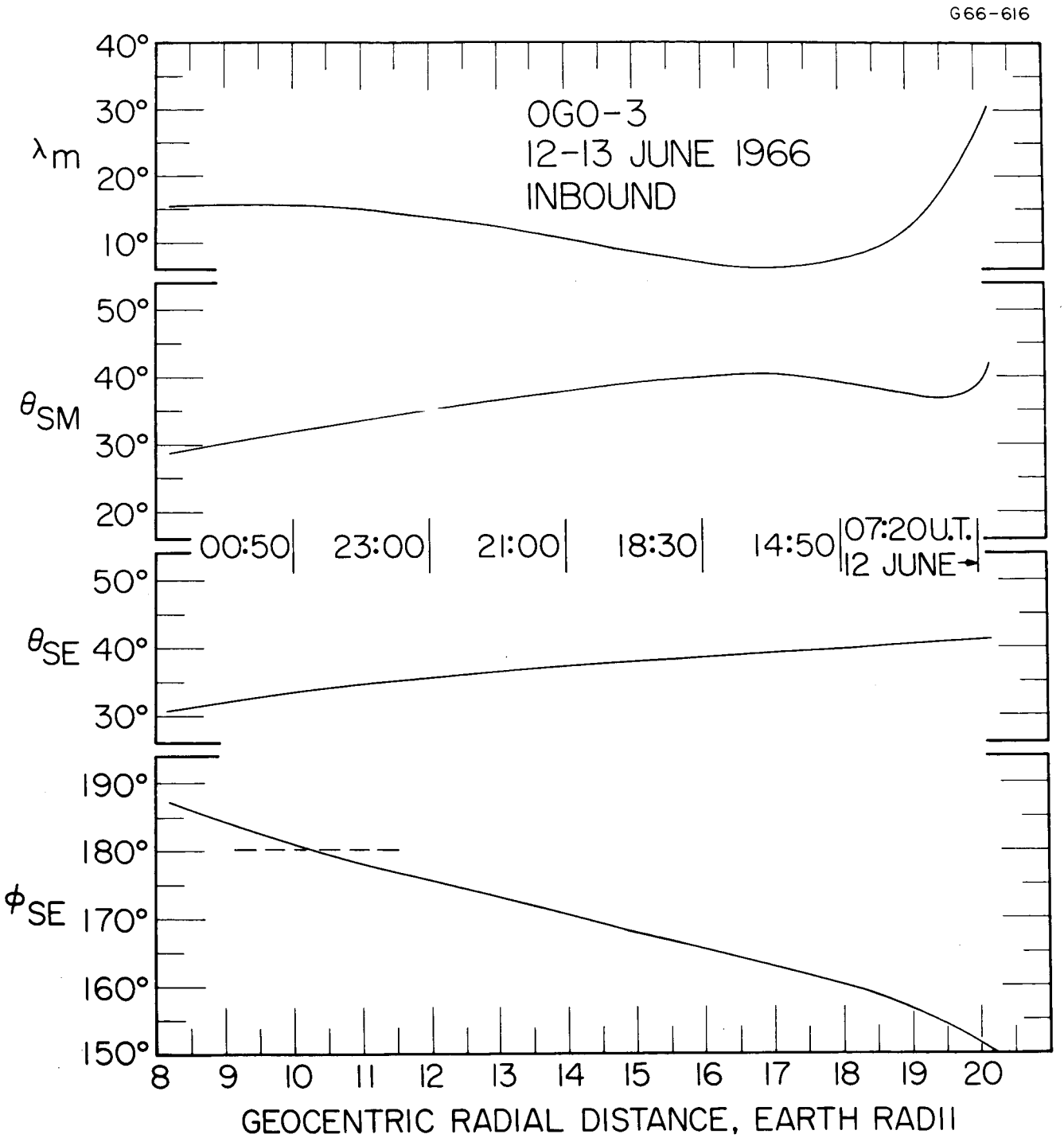
G66-616
OGO-3
12-13 JUNE 1966
INBOUND
λm
θSM
θSE
φSE
40°
30°
20°
10°
50°
40°
30°
20°
00:50
23:00
21:00
18:30
14:50
07:20 U.T.
12 JUNE
50°
40°
30°
190°
180°
170°
160°
150°
8
9
10
11
12
13
14
15
16
17
18
19
20
GEOCENTRIC RADIAL DISTANCE, EARTH RADII

Figure 5

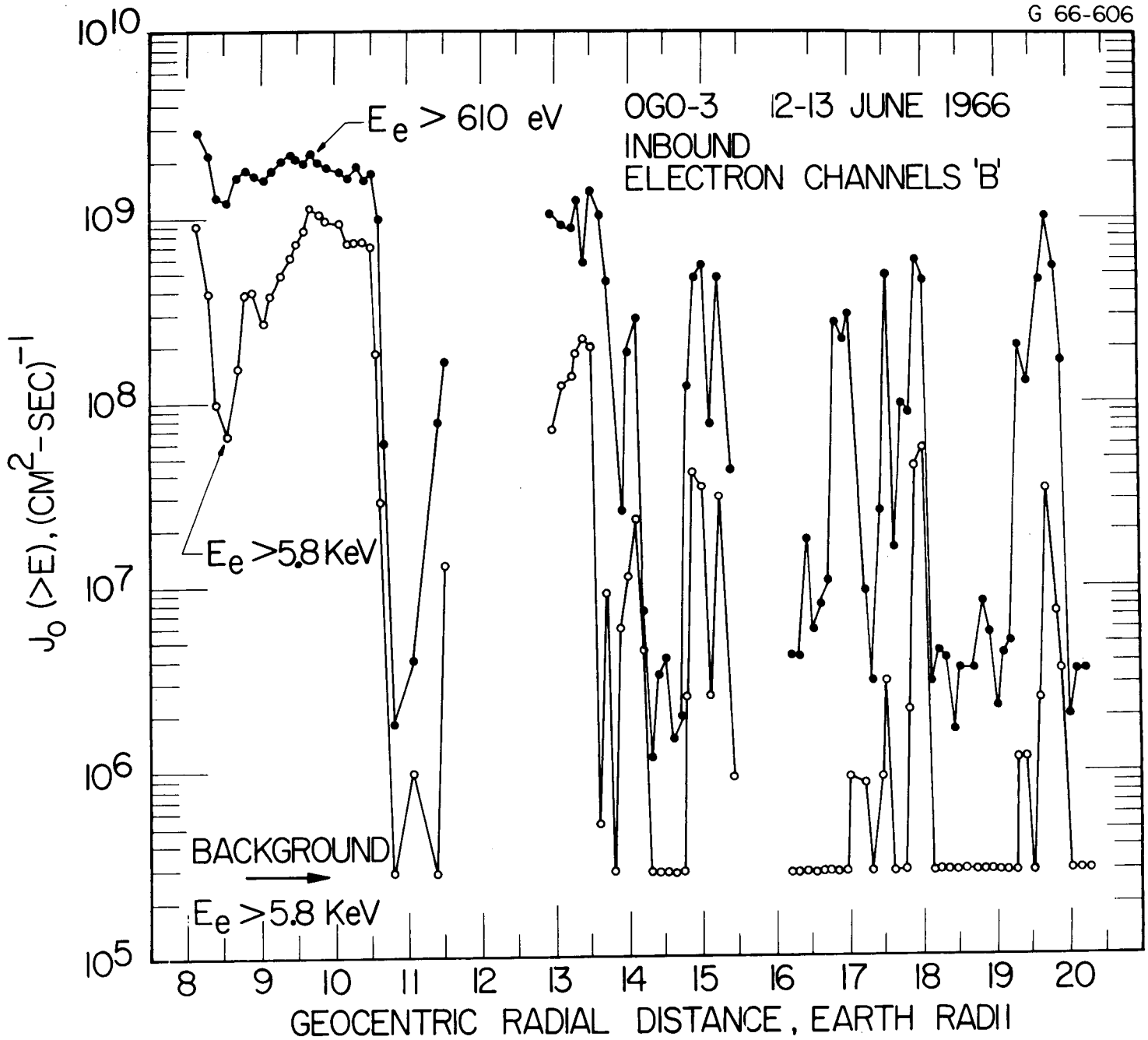
G 66-606
OGO-3 12-13 JUNE 1966
INBOUND
ELECTRON CHANNELS 'B'
$E_e > 610$ eV
$E_e > 5.8$ KeV
BACKGROUND
$E_e > 5.8$ KeV
$J_o (>E), (CM^2-SEC)^{-1}$
10^{10}
10^9
10^8
10^7
10^6
10^5
8 9 10 11 12 13 14 15 16 17 18 19 20
GEOCENTRIC RADIAL DISTANCE, EARTH RADII

Figure 6

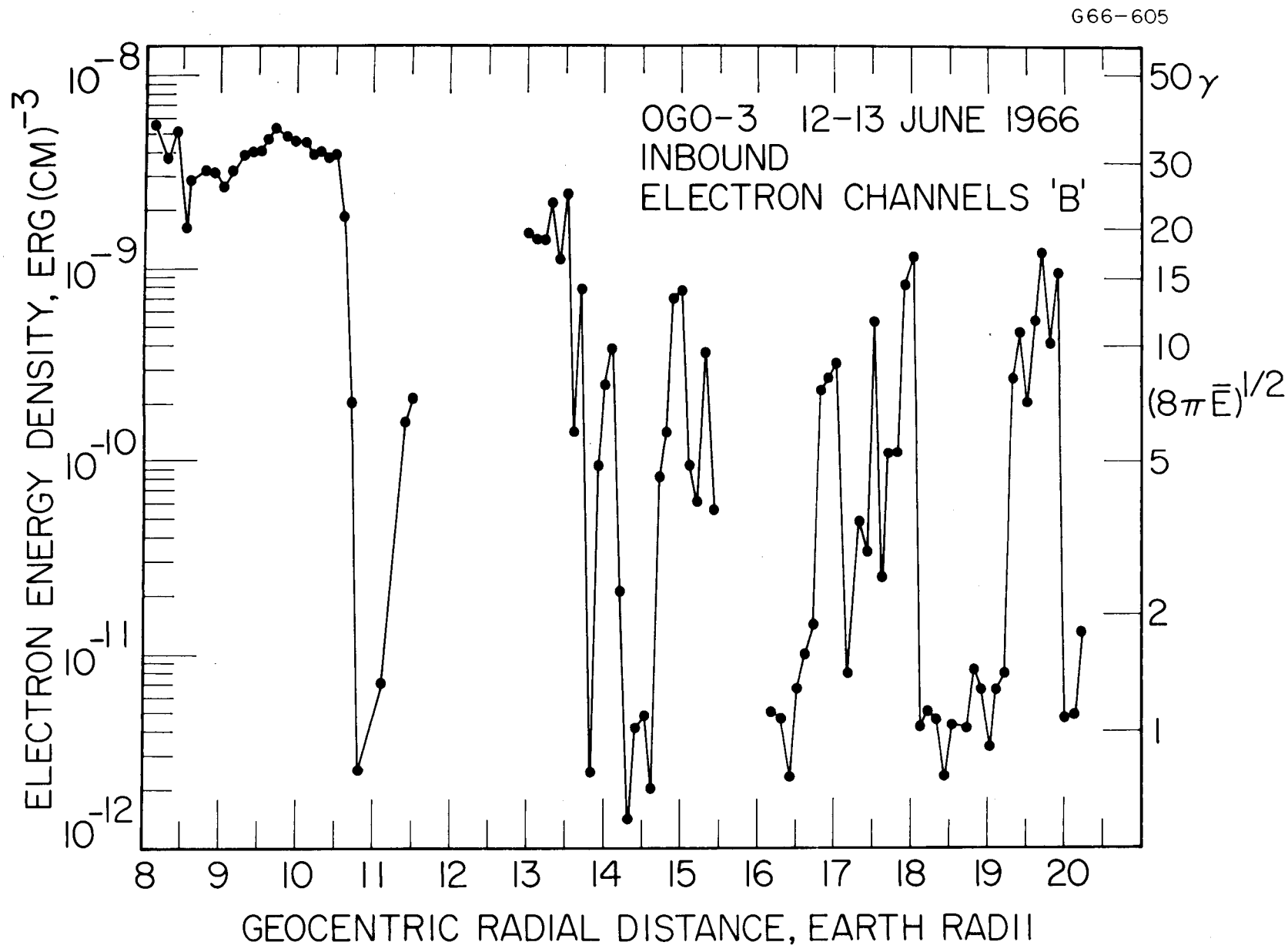
G66-605
OGO-3 12-13 JUNE 1966
INBOUND
ELECTRON CHANNELS 'B'
ELECTRON ENERGY DENSITY, ERG (CM)$^{-3}$
10^{-8}
10^{-9}
10^{-10}
10^{-11}
10^{-12}
50 γ
30
20
15
10
$(8\pi \bar{E})^{1/2}$
5
2
1
8 9 10 11 12 13 14 15 16 17 18 19 20
GEOCENTRIC RADIAL DISTANCE, EARTH RADII

Figure 7

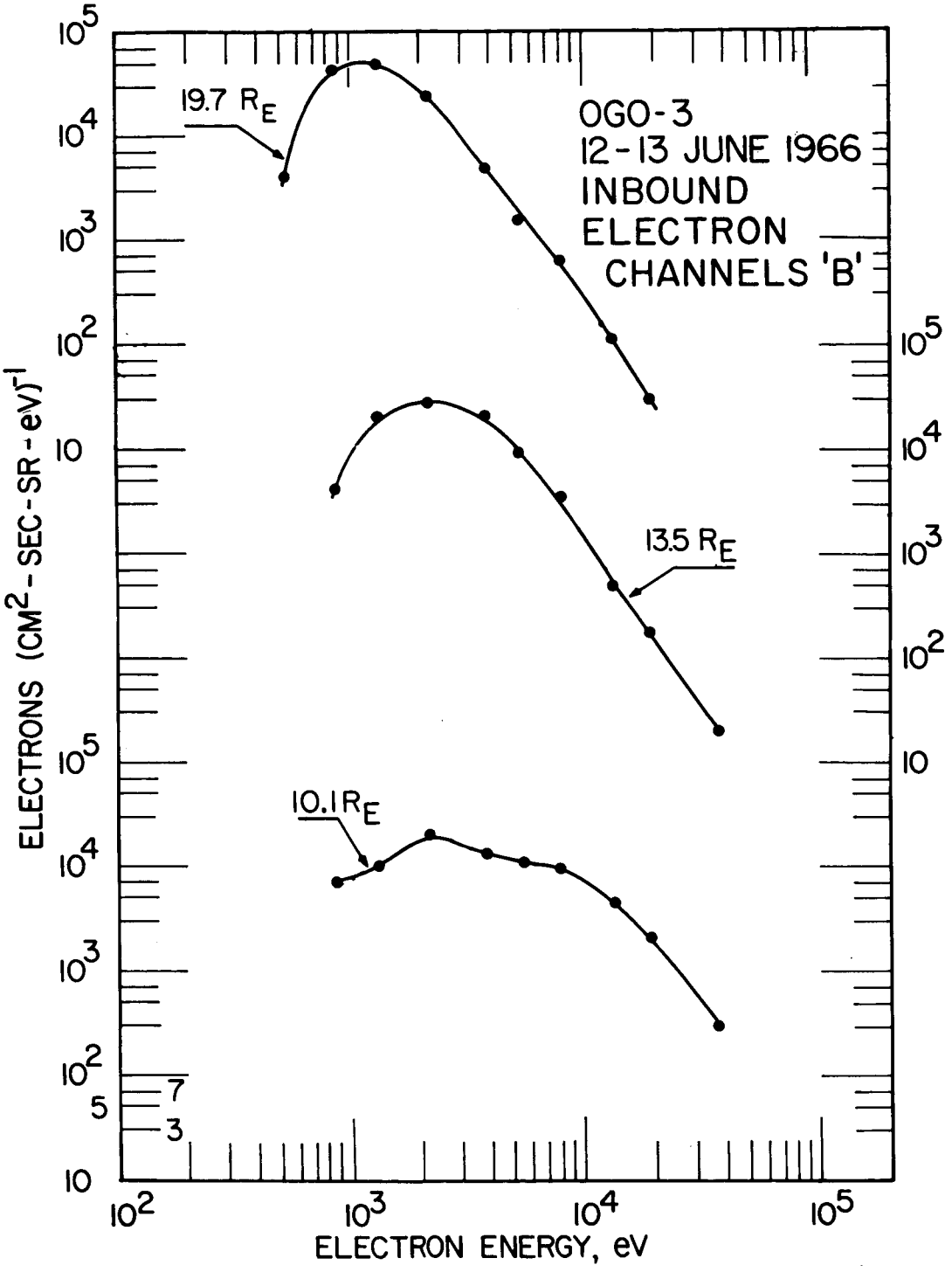
OGO-3
12-13 JUNE 1966
INBOUND
ELECTRON
CHANNELS 'B'
19.7 R_E
13.5 R_E
10.1 R_E
ELECTRONS (CM^2-SEC-SR-eV)$^{-1}$
ELECTRON ENERGY, eV
10^5
10^4
10^3
10^2
10
7
5
3

Figure 8

G 66-591

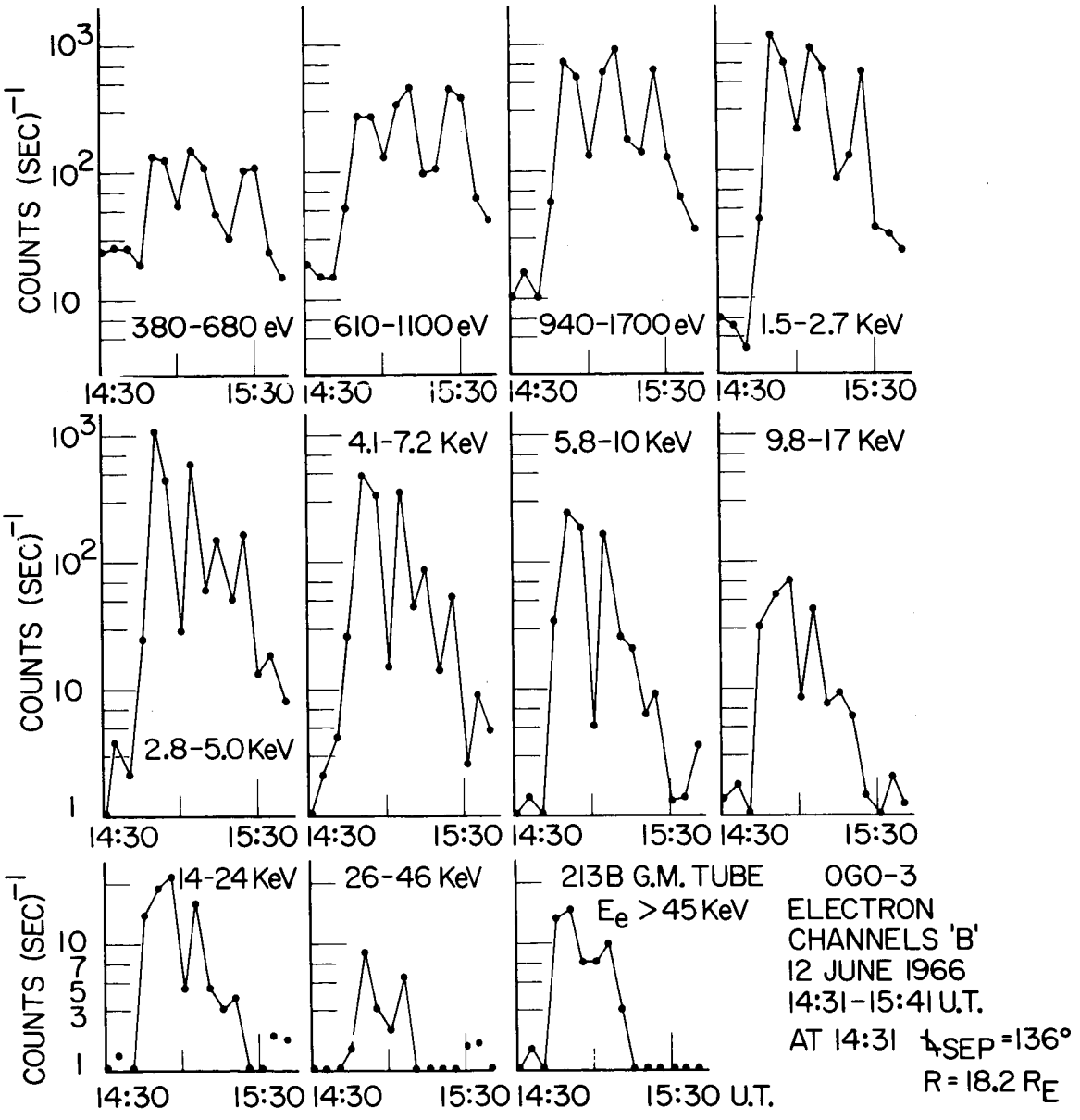

Figure 9

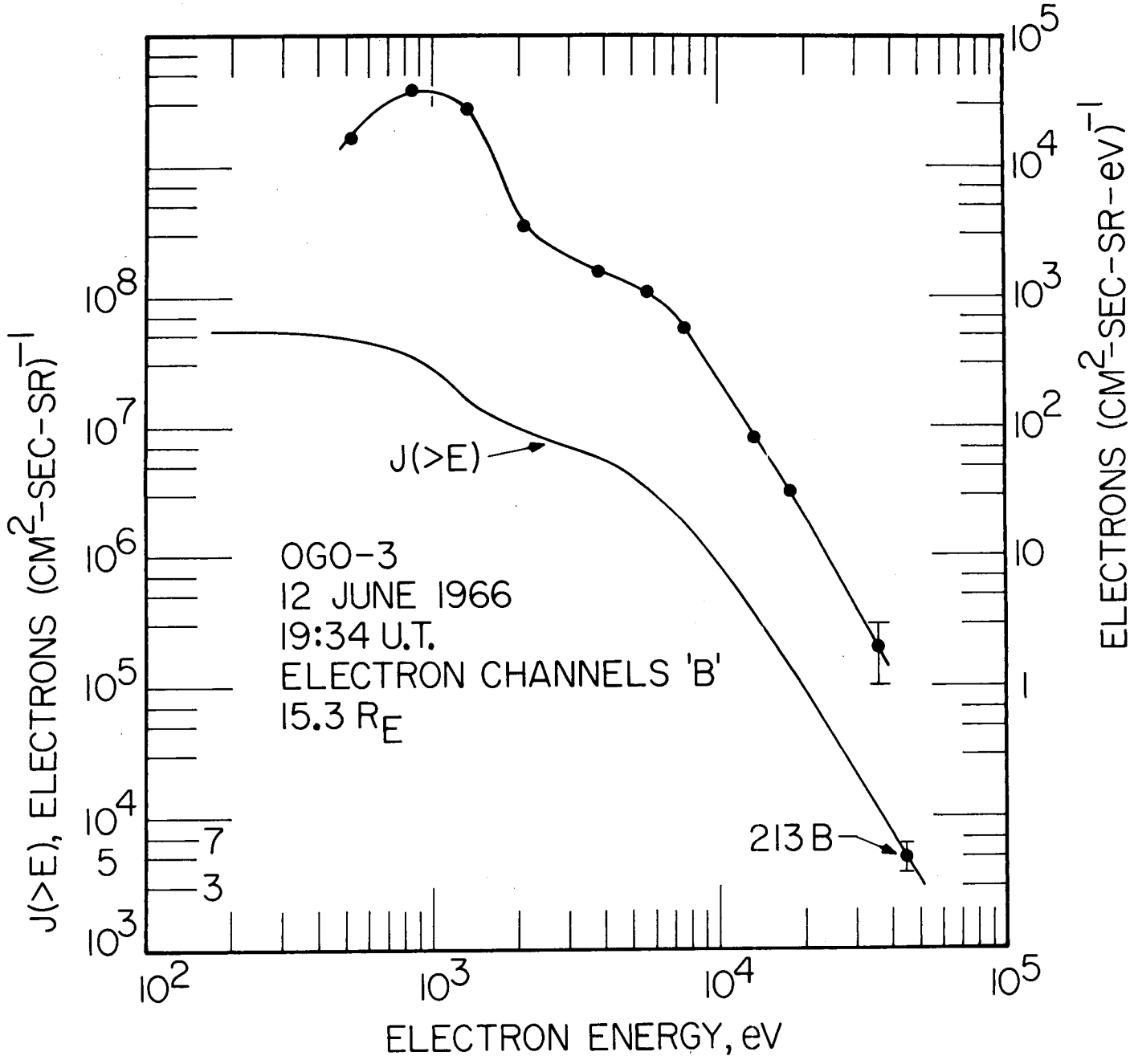
J(>E), ELECTRONS (CM²-SEC-SR)⁻¹
ELECTRONS (CM²-SEC-SR-eV)⁻¹
ELECTRON ENERGY, eV
J(>E)
OGO-3
12 JUNE 1966
19:34 U.T.
ELECTRON CHANNELS 'B'
15.3 R_E
213 B
10⁸
10⁷
10⁶
10⁵
10⁴
7
5
3
10³
10⁵
10⁴
10³
10²
10
1
10²
10³
10⁴
10⁵

Figure 10

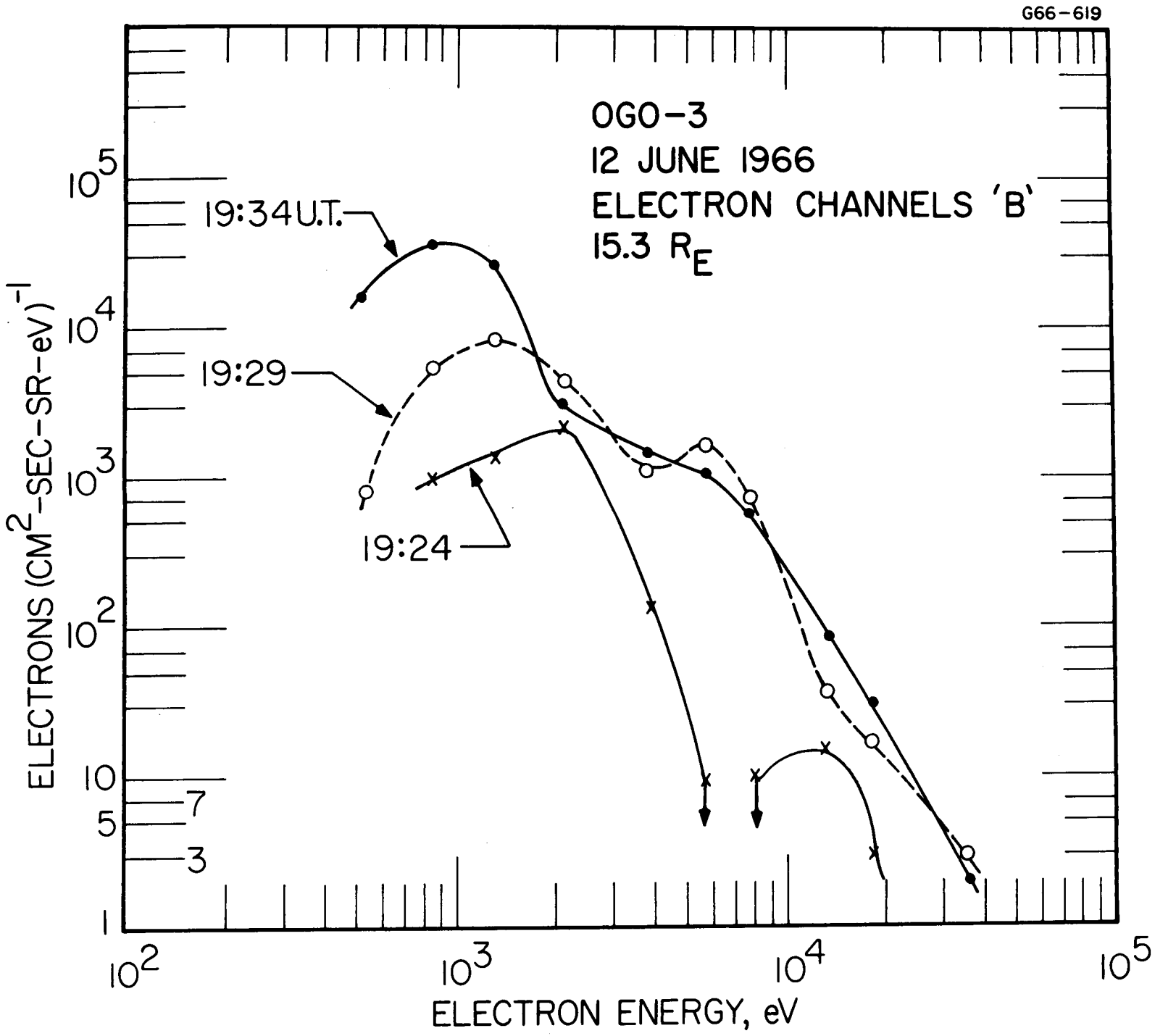
G66-619
OGO-3
12 JUNE 1966
ELECTRON CHANNELS 'B'
15.3 R_E
19:34 U.T.
19:29
19:24
ELECTRONS (CM^2-SEC-SR-eV)$^{-1}$
10^5
10^4
10^3
10^2
10
7
5
3
1
10^2
10^3
10^4
10^5
ELECTRON ENERGY, eV

Figure 11

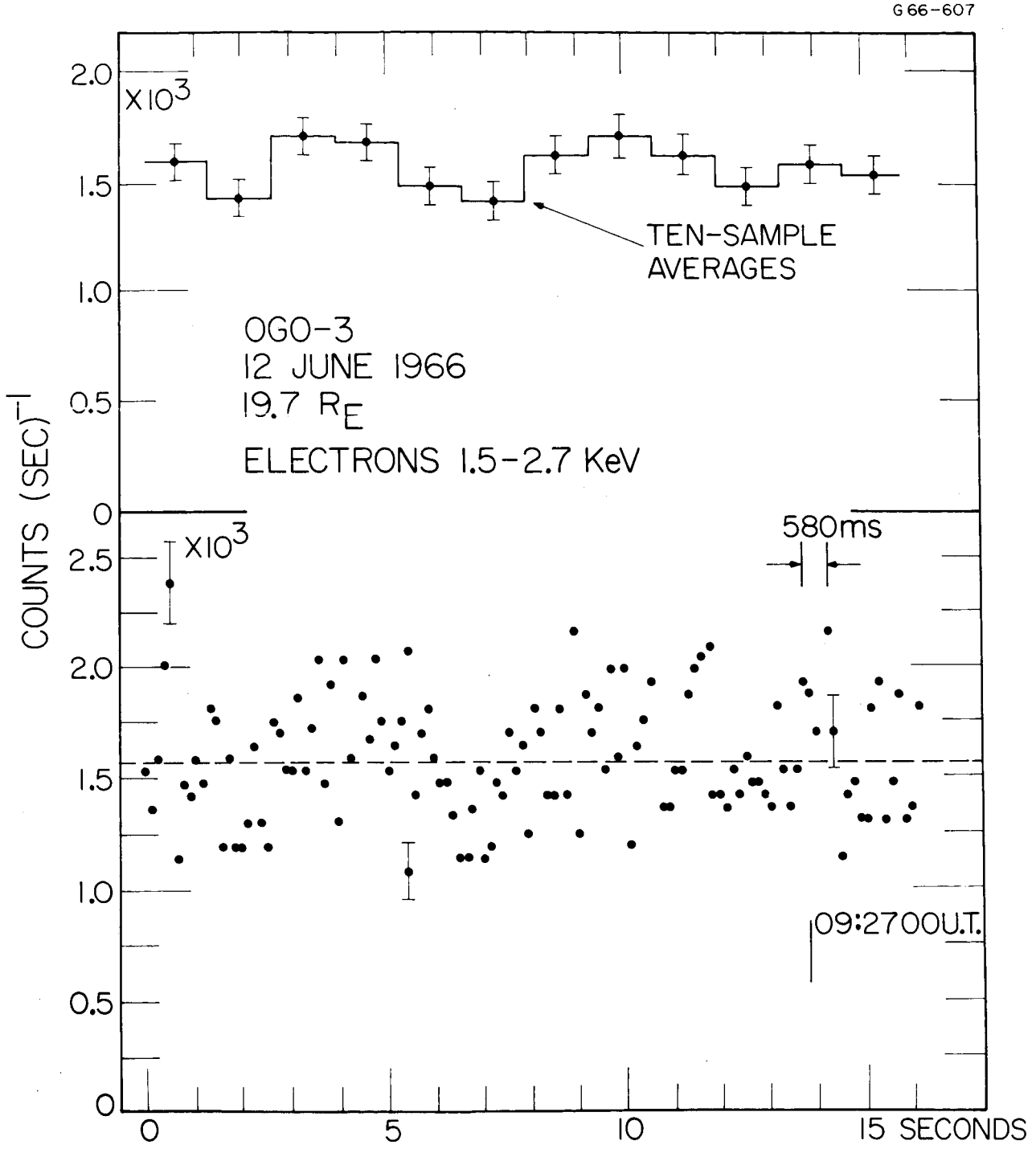
G 66-607
X10^3
TEN-SAMPLE AVERAGES
OGO-3
12 JUNE 1966
19.7 R_E
ELECTRONS 1.5-2.7 KeV
X10^3
580ms
09:27 00 U.T.
COUNTS (SEC)^-1
2.0
1.5
1.0
0.5
0
2.5
0
5
10
15 SECONDS

Figure 12

UNCLASSIFIED
Security Classification

DOCUMENT CONTROL DATA - R&D
(Security classification of title, body of abstract and indexing annotation must be entered when the overall report is classified)

1. ORIGINATING ACTIVITY (Corporate author)	2a. REPORT SECURITY CLASSIFICATION
University of Iowa, Department of Physics and Astronomy	UNCLASSIFIED
	2b. GROUP

3. REPORT TITLE

Initial Observations of Low-Energy Electrons in the Earth's Magnetosphere with OGO 3

4. DESCRIPTIVE NOTES (Type of report and inclusive dates)

Progress August 1966

5. AUTHOR(S) (Last name, first name, initial)

Frank, L. A.

6. REPORT DATE	7a. TOTAL NO. OF PAGES	7b. NO. OF REFS
August 1966	48	17

8a. CONTRACT OR GRANT NO.	9a. ORIGINATOR'S REPORT NUMBER(S)
b. PROJECT NO.	U. of Iowa 66-39
c.	9b. OTHER REPORT NO(S) (Any other numbers that may be assigned this report)
d.	

10. AVAILABILITY/LIMITATION NOTICES

Qualified requesters may obtain copies of this report from DDC.

11. SUPPLEMENTARY NOTES	12. SPONSORING MILITARY ACTIVITY
	Office of Naval Research

13. ABSTRACT

Initial observations of electrons over the energy range extending from ~ 100 eV to 50 keV at geocentric radial distances 8 R_E to 20 R_E in the dark hemisphere of the earth's magnetosphere with electrostatic analyzers borne on OGO 3 (launch, 7 June 1966) are presented for the inbound pass of the satellite on 12-13 June 1966. The electron differential energy spectrums typically are characterized by a single peak in intensities occurring in the energy range ~ 0.8 to 10 keV and at lower energies with increasing geocentric radial distances, by broader width with decreasing radial distance, and by greater slopes for electron energies $E_e \gtrsim 5$ keV with increasing radial distance. The radial profiles of unidirectional and omnidirectional, integral and differential intensities, and energy densities of electrons within the above energy range are characterized by catastrophic variations in magnitude which are presumably reflections of both temporal and spatial variations in intensities. A relatively uncommon example of an electron spectrum with two peaks in intensity at $E_e \sim 1$ keV and ~ 10 keV is examined during the onset of the event and the peaks in electron intensity were found to occur at lower energies with increasing time. Beyond ~ 13 R_E many electron spectrums are 'monoenergetic' to the extent that $\gtrsim 75\%$ of the energy flux is shared among electrons in the energy range 1 to 3 keV although measurable electron intensities are observed over the entire energy range ~ 500 eV to 50 keV. In contrast with the presistent softening of the electron spectrums with increasing radial distance 8 to 20 R_E, the electron energy densities in the peaks of intensities do not show a marked radial dependence beyond ~ 13 R_E. The

DD FORM 1 JAN 64 1473

UNCLASSIFIED
Security Classification

Continuation of Item 13, ABSTRACT:

observed electron ($E_e > 610$ eV) energy densities in the peaks of the radial profiles almost always rise to $\sim 10^{-9}$ erg(cm)$^{-3}$, an effect which may be indicative of an instability of 'saturation' of the local magnetic field, and are significant in substantially distorting the geomagnetic field beyond ~ 8 R_E. Typical values of the ratios of intensities $J(E_e > 610$ eV)/ $J(E_e > 45$ keV) are typically 10^4 in the magnetospheric tail. The maximum temporal resolution of the apparatus in $\sim$ 100 milliseconds: temporal variations in low-energy electron intensities by factors $\gtrsim 2$ occur usually in periods $\sim$ seconds to several minutes.

14. KEY WORDS	LINK A		LINK B		LINK C	
	ROLE	WT	ROLE	WT	ROLE	WT
Magnetosphere						
Auroral Zone						
Natural Radiation Belts						
Van Allen Radiation						

INSTRUCTIONS

1. ORIGINATING ACTIVITY: Enter the name and address of the contractor, subcontractor, grantee, Department of Defense activity or other organization *(corporate author)* issuing the report.

2*a*. REPORT SECURITY CLASSIFICATION: Enter the overall security classification of the report. Indicate whether "Restricted Data" is included. Marking is to be in accordance with appropriate security regulations.

2*b*. GROUP: Automatic downgrading is specified in DoD Directive 5200.10 and Armed Forces Industrial Manual. Enter the group number. Also, when applicable, show that optional markings have been used for Group 3 and Group 4 as authorized.

3. REPORT TITLE: Enter the complete report title in all capital letters. Titles in all cases should be unclassified. If a meaningful title cannot be selected without classification, show title classification in all capitals in parenthesis immediately following the title.

4. DESCRIPTIVE NOTES: If appropriate, enter the type of report, e.g., interim, progress, summary, annual, or final. Give the inclusive dates when a specific reporting period is covered.

5. AUTHOR(S): Enter the name(s) of author(s) as shown on or in the report. Enter last name, first name, middle initial. If military, show rank and branch of service. The name of the principal author is an absolute minimum requirement.

6. REPORT DATE: Enter the date of the report as day, month, year; or month, year. If more than one date appears on the report, use date of publication.

7*a*. TOTAL NUMBER OF PAGES: The total page count should follow normal pagination procedures, i.e., enter the number of pages containing information.

7*b*. NUMBER OF REFERENCES: Enter the total number of references cited in the report.

8*a*. CONTRACT OR GRANT NUMBER: If appropriate, enter the applicable number of the contract or grant under which the report was written.

8*b*, 8*c*, & 8*d*. PROJECT NUMBER: Enter the appropriate military department identification, such as project number, subproject number, system numbers, task number, etc.

9*a*. ORIGINATOR'S REPORT NUMBER(S): Enter the official report number by which the document will be identified and controlled by the originating activity. This number must be unique to this report.

9*b*. OTHER REPORT NUMBER(S): If the report has been assigned any other report numbers *(either by the originator or by the sponsor)*, also enter this number(s).

10. AVAILABILITY/LIMITATION NOTICES: Enter any limitations on further dissemination of the report, other than those imposed by security classification, using standard statements such as:

(1) "Qualified requesters may obtain copies of this report from DDC."

(2) "Foreign announcement and dissemination of this report by DDC is not authorized."

(3) "U. S. Government agencies may obtain copies of this report directly from DDC. Other qualified DDC users shall request through _____."

(4) "U. S. military agencies may obtain copies of this report directly from DDC. Other qualified users shall request through _____."

(5) "All distribution of this report is controlled. Qualified DDC users shall request through _____."

If the report has been furnished to the Office of Technical Services, Department of Commerce, for sale to the public, indicate this fact and enter the price, if known.

11. SUPPLEMENTARY NOTES: Use for additional explanatory notes.

12. SPONSORING MILITARY ACTIVITY: Enter the name of the departmental project office or laboratory sponsoring *(paying for)* the research and development. Include address.

13. ABSTRACT: Enter an abstract giving a brief and factual summary of the document indicative of the report, even though it may also appear elsewhere in the body of the technical report. If additional space is required, a continuation sheet shall be attached.

It is highly desirable that the abstract of classified reports be unclassified. Each paragraph of the abstract shall end with an indication of the military security classification of the information in the paragraph, represented as *(TS)*, *(S)*, *(C)*, or *(U)*.

There is no limitation on the length of the abstract. However, the suggested length is from 150 to 225 words.

14. KEY WORDS: Key words are technically meaningful terms or short phrases that characterize a report and may be used as index entries for cataloging the report. Key words must be selected so that no security classification is required. Identifiers, such as equipment model designation, trade name, military project code name, geographic location, may be used as key words but will be followed by an indication of technical context. The assignment of links, roles, and weights is optional.